HERBERT C. CARLSON

THE HILAT GROUND-BASED PROGRAM

The comprehensive complement of HILAT in situ measurements requires a complementary global set of ground-based measurements to address the HILAT objective rigorously: understanding high-latitude plasma structure. The rationale for and the nature of the ground-based diagnostics are presented, identifying within an integrated program the roles of coherent and incoherent scatter radars, radio beacon receivers, Fabry-Perot interferometers, and all-sky image-intensified optical sensors.

OBJECTIVE

The HILAT program seeks to understand high-latitude plasma structures over the extreme range of scale sizes from thousands of kilometers down to meters. Theory and experiment have mutually matured to the stage where this goal is realistic. Realization requires physical models of microscale processes, geophysical models of global scale-processes, and simultaneous comprehensive diagnostics. An existing theoretical framework identifies both the complement of measurements and the vast range of scale sizes (approximately 100 km to ion gyro radius) that must be simultaneously measured. Nonlinear interactions lead large-scale structures to produce smaller scales, which may ultimately be dissipated by still finer scale structures. The HILAT polar-orbiting satellite measures the particles, fields, and currents that can lead to high-latitude irregularity formation, simultaneously with direct radio beacon observations of results of phase and amplitude scintillation over the radio frequency range of principal concern.

This must be complemented by comprehensive ground-based measurements to trace the time history critical to scintillation development, to determine horizontal and vertical spatial coupling, and to determine geometrical intensification effects. Coupling among different spatial regions, different processes, and structures of different sizes must be traced during seeding, evolution, transport, and dissipation of plasma structure.

Theory and experiment must each be judged within their mutually interactive framework.

EXPERIMENTAL REQUIREMENTS

Our current view of high-latitude plasma structure leads to the following set of experimental requirements:

1. Parameters (comprehensive simultaneous diagnostics to isolate alternative processes),
2. Wavelength (complementary diagnostics for less than 10 meters to 100 km or more),
3. Space (2-D or 3-D sampling to track spatial coupling),
4. History (time continuity to trace evolution, growth, and decay),
5. Geometry (2-D or 3-D sampling/spaced receivers for geomagnetic control/aspect sensitivity).

These requirements emerge from the following geophysical considerations.

BACKGROUND

Geophysical Considerations

Electron concentration and electric field data from high-inclination satellites demonstrate that the entire polar cap and auroral regions of the ionosphere are characterized by a broad spectrum of irregularities (typically between 100 km and 10 meters) and that this region is usually bounded in latitude by a sharp transition to a smooth lower latitude ionosphere. Amplitude and phase scintillation data obtained within the polar cap and auroral region demonstrate that strong scintillation (a direct consequence of spatial structure of the integrated electron density deviation in the line of sight) may be seen 24 hours a day under special conditions at these high latitudes.

These scintillations are currently thought to arise as follows. A large-scale structure (greater than 100 km) in the high-latitude plasma will form as a direct consequence of a large-scale transport and chemical effects on plasma initially produced by solar radiation at high and upper mid-latitudes and/or particle precipitation at high latitudes. Free-energy sources drive various plasma instabilities leading to smaller size structure (approximately 100 km through submeter). The free-energy sources include ionospheric plasma density (n_e) gradients, electric fields **(E)**, plasma velocity **(V)** shears, currents **(I)** parallel or perpendicular to the earth's magnetic field **(B)**, and perhaps neutral atmospheric winds **(U)** or even neutral atmospheric turbulence. The plasma instabilities may be either directly forced (e.g., $\mathbf{E} \times \mathbf{B}$ or gradient drift, current convective; see the article by Keskinen in this issue) or indirectly generated (e.g., wave-wave, cascading). Ultimately, this is limited and quenched by diffusive processes, whether wave particle diffusion or "anomalous" diffusion. These instability processes in-

volve nonlinear interactions that can couple between different wavelength structures.

Isolation of the key free-energy sources and the dominant instability processes then requires simultaneous measurement of the baseline value and turbulent structure in **E** or **V**, plasma density and temperature, **U** to define the rest frame for **E** and **V**, thermal and energetic particle components of **I**, energetic particle fluxes, and scintillation (scintillation being a sensitive measure of the degree of fluctuation of integrated irregularity electron density deviation along the line of sight). The nonlinear coupling between structures of different wavelengths requires sampling a dynamic range exceeding 10^5 in scale size (greater than 100 km through submeter) to address present instability theory questions.

High-latitude plasma is produced by energetic particles (particularly electrons) through impact ionization of the upper atmosphere. Both the ion production rate and its altitude depend sensitively on the particle energy. Electrons of energy exceeding 1 kiloelectronvolt (keV) produce ionization (one ion-electron pair per 35 eV) near and below 110 km, in the ionospheric E region; those with energies less than 500 eV produce ionization (one ion-electron pair per 50 to 60 eV) above 200 km in the F region. If in sunlight, this ionization production is augmented by solar radiation. Chemical lifetimes in the E region are seconds to minutes, and thus E-region plasma distributions closely track temporal-spatial structure in the particle flux exceeding 1 keV. Chemical lifetimes in the F region are hours to a day, during which time the magnetically confined volume of plasma in question may travel thousands of kilometers across the polar, auroral, and even upper mid-latitude regions of the globe. Thus F-region bulk plasma density (100 to 1000 km scale) represents the integrated effects of production and chemical loss over its itinerant lifetime. The instantaneous (as observed by HILAT) spectral properties of finer structure within it similarly represent the integrated consequence of exposure to conditions of various instabilitiy growth and decay rates operating on the moving bulk plasma.

Certain formation processes should lead to F-region structure elongated in favored directions (e.g., aligned along surfaces of constant magnetic latitude, called "L-shell aligned," or aligned along plasma or convection flow lines) in addition to being magnetic field aligned.

Patterns of Dynamics

The high-latitude ionosphere is extremely dynamic as well as quite structured. A few patterns of motion should be identified here.

Episodes of strongly enhanced VHF scintillation (20 decibels peak-to-peak fluctuations) are found in the polar cap, against a lower persistent background level. Dedicated Air Force Geophysics Laboratory aircraft field programs[1,2] established two patterns in space and time (Fig. 1) for these severe plasma-structuring events: (a) during magnetically quiet times (B_z northward), sun-aligned walls of F-region ionization (sensed by ionosonde echoes up to 6 to 10 megahertz and generating severe scintillations) are produced by ongoing intense fluxes of the order of 100 eV electrons and exhibit drifts of approximately 0 to 250 meters per second across the pole, generally from dawn toward dusk; and (b) during magnetically disturbed times (B_z southward), patches of strongly enhanced (about 5 to 10 times the background level) but decaying F-region ionization, generating severe scintillation, drift across the pole from noon toward midnight at speeds of 0.25 to nearly 1 km/second. Each of these phenomena identifies and impels specific scientific studies necessary to the understanding of high-latitude plasma structuring and scintillation. Another region of regular scintilla-

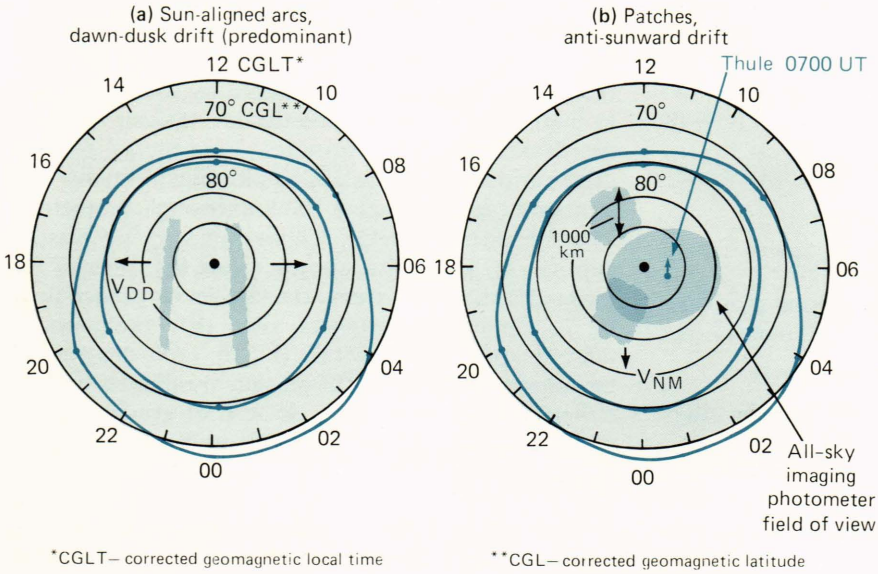

*CGLT– corrected geomagnetic local time

**CGL– corrected geomagnetic latitude

Figure 1 — Patterns of motion of polar cap F-region structures (a) during magnetically quiet times and (b) during magnetically disturbed periods.[2]

tion occurrence is found in the auroral oval and will be discussed in connection with Fig. 10; its magnitude is greatly enhanced during substorms, as shown in Fig. 6.[3]

The bulk F-region plasma horizontal velocity at high latitudes, though structured, generally shows reasonable conformity (for B_z southward) to a double cell "convection pattern" such as shown in Fig. 2a. The plasma flows away from the sun across the polar cap, through the midnight sector, and by continuity returns sunward at lower latitudes, through either the dawn or dusk sector, as shown by the arrows on the flow lines in Fig. 2a. One thinks in terms of "convecting" tubes of magnetic flux, confining a volume within which plasma is continually being lost on the bottomside by recombination (and, in restricted regions of space and time, out the top when sufficiently energized to escape the earth's gravitational pull), and replenished by solar radiation and energetic particle production. Since the plasma flow velocity $\mathbf{V} = \mathbf{E} \times \mathbf{B}$, this is a measure of the potential drop across the polar cap (55 kilovolts in this example) imposed by the interaction of the earth's distant magnetic field (magnetosphere) with the solar wind. The size of the pattern depends on a number of factors, including the velocity of the solar wind and the direction of the interplanetary magnetic field. Significant localized and circumpolar fluctuations can occur over time periods of an hour or less. These **E** patterns drive global-scale motion of bulk plasma within which a structure preexists, or they can generate plasma density irregularities through the $\mathbf{E} \times \mathbf{B}$ instability.

The background atmosphere at F-region altitudes, the thermosphere, is not a simple fixed frame of reference within which instabilities form. The thermosphere itself is in a state of motion sufficiently rapid to be of concern here. Polar flow calculated for a representative ionospheric condition similar to that of Fig. 2a is shown in Fig. 2b. In the early to mid 1970's, thermospheric circulation was thought to be dominated by simple flow from a subsolar hot spot (high-pressure area) to an antisolar cold spot. By the late 1970's, it became recognized that significant "back pressures" can be generated by highly variable auroral particle and auroral current heating, which can transiently (in space and time) exceed solar heating (0.5 erg per centimeter-second above 110 km) by 100 times. (Note the variability discussed in connection with Fabry-Perot interferometers and illustrated in Fig. 5 for Calgary, Alberta.) Momentum transfer from plasma convecting through the thermosphere imparts a further variable stirring effect. The time required for a neutral particle to suffer an ion-to-neutral momentum-transfer collision is simply linearly proportional to the concentration of ions present: at F-region altitudes, this time scale is a quarter of a day for modest plasma densities of 10^5 per cubic centimeter and half an hour for relatively high densities of 10^6 per cubic centimeter. This is the driver for the polar pair of cells in Fig. 2b, as might be suggested by comparison with Fig. 2a.

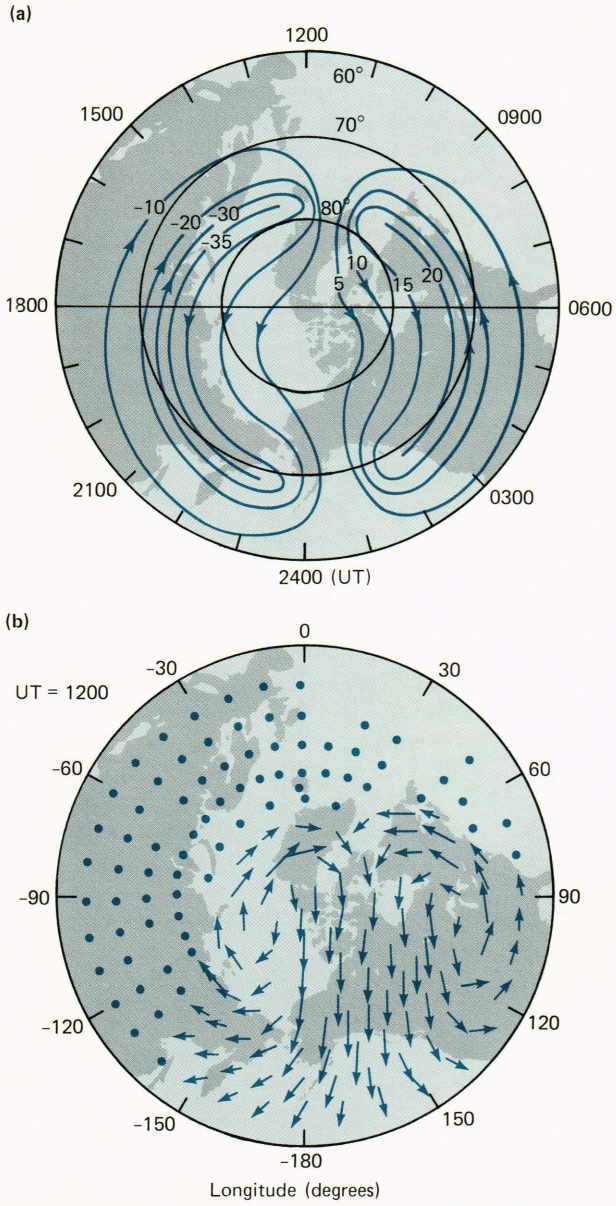

Figure 2 — (a) Model of flow patterns of high-latitude F-region plasma and thermosphere (Empirical convection model based on Atmosphere Explorer satellite data.) It takes into account convection features such as the dayside throat and the harang discontinuity.[5] (b) Polar plots of the calculated circulation over the northern hemisphere polar region during late October for the case of solar heating plus magnetospheric convection with a cross-tail potential of 60 kilovolts. The geomagnetic and geographic poles are displaced and the circulation is at 1200 universal time (UT).[6]

GROUND-BASED MEASUREMENTS PROGRAM

The fields of view of many optical, radio, and radar facilities important to the HILAT mission are

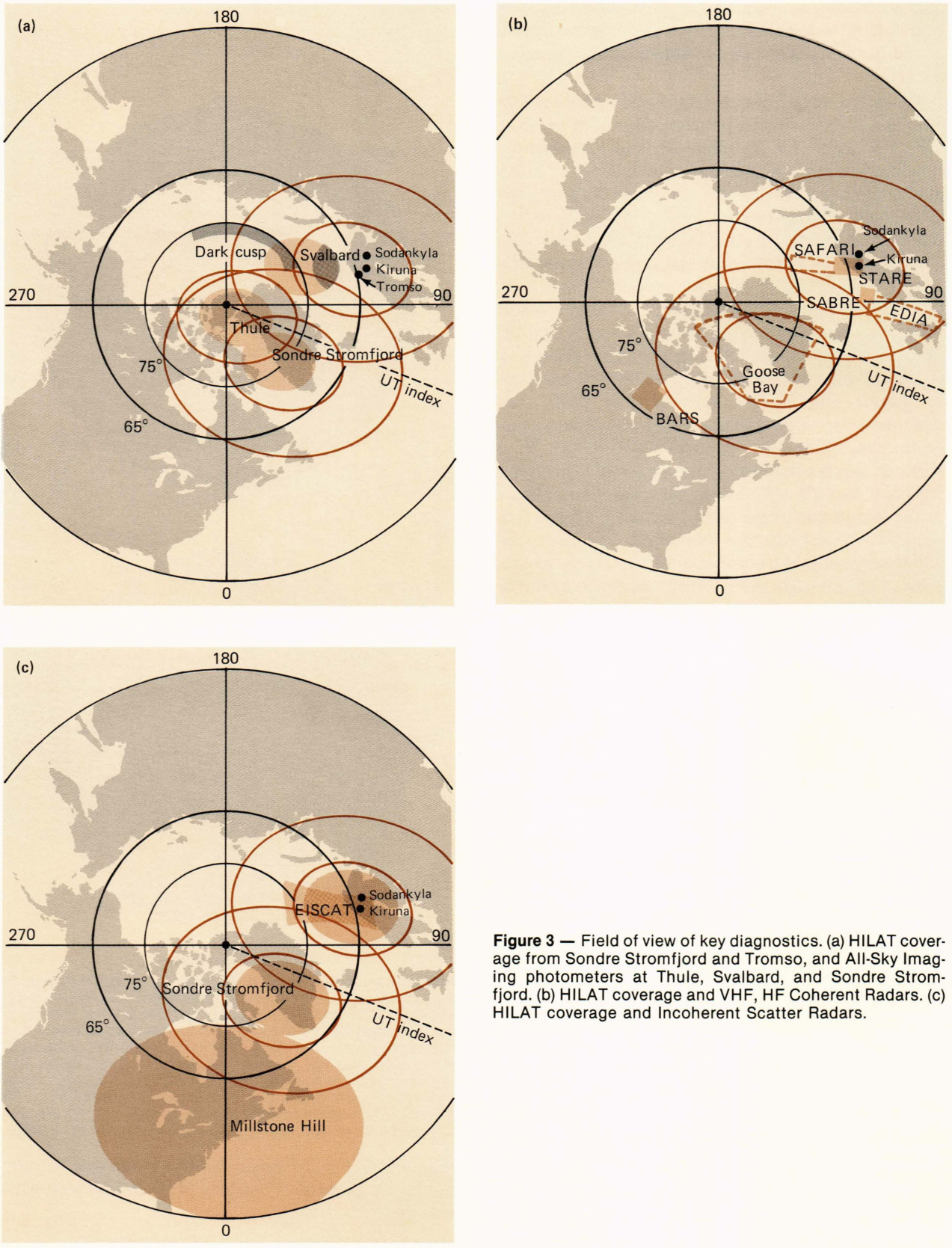

Figure 3 — Field of view of key diagnostics. (a) HILAT coverage from Sondre Stromfjord and Tromso, and All-Sky Imaging photometers at Thule, Svalbard, and Sondre Stromfjord. (b) HILAT coverage and VHF, HF Coherent Radars. (c) HILAT coverage and Incoherent Scatter Radars.

shown in Fig. 3. The polar projection maps shown in Fig. 3 have been reconformed to allow contours of constant geomagnetic latitude to appear as concentric circles about the geomagnetic pole (the geographic pole

is labeled NP). The 75° and 65° geomagnetic latitude circles are drawn explicitly. Circular fields of view of ground-based instruments appear as ellipses. Consecutive HILAT ground traces would be a series of transpolar lines separated by about 25° of longitude under the orbital plane and tangent to a geographic "circle" 7.8° from the geographic north pole.

In Fig. 3, large and small solid line ellipses, centered on the two HILAT receiving station sites at Sondre Stromfjord, Greenland, and at Tromso, Norway, have been repeated. The large ellipse represents the HILAT in situ field of view at 830 km altitude, covering cusp-polar regions from Sondre Stromfjord and auroral-plasmapause regions from Tromso. This combination affords comprehensive coverage of regions of concern. Each site was motivated by proximity to an incoherent scatter radar diagnostic, each with a clustering of associated supporting diagnostics. The smaller ellipses represent a radio beacon scintillation field of view of these two receiving sites, assuming a typical F-region height of 300 km. Further descriptions of Fig. 3 are provided in the following section.

Optical Diagnostics

All-Sky Imaging Photometers. Figure 3a shows as shaded ellipses the fields of view of three all-sky imaging photometers dedicated to support the HILAT mission from Thule, Svalbard, and Sondre Stromfjord. Each has a 155° field of view (spanning 1200 km for F-region emissions), a 30 Rayleigh (1 Rayleigh = 10^6 photons/cm^2 second) threshold sensitivity, a 10^2 dynamic range on film or TV recorder, and a 10 second time resolution, but a typical 0.5 to 2 minute time to cycle through two to four filter wavelengths usually including 4278 angstrom (1 Å = 10^{-10} meters) N_2^+, 5577 Å, 6300 Å OI, and 7320 Å OII. By October 1984, an airborne all-sky imaging photometer will employ charge- coupled device technology to offer 10^5 dynamic range, spanning recombination to auroral intensities in the same field of view.

The strong polar scintillation patterns discussed in connection with Fig. 1 made it clear that, in contrast to the north-south/east-west orientation of auroral and lower latitude studies, in very-high-latitude regions the most useful geometric frame of reference is more nearly the sun-earth line, i.e., noon-midnight and dawn-dusk. The polar network of all-sky image-intensified optical sensors of Fig. 3a has been deployed in large part to provide a frame of reference for interpreting HILAT and associated ground-based data.

Intensified images of the 6300 Å atomic oxygen line track transpolar motion of regions of significant scintillation over the polar cap. These are associated with both weak recombination emission of F-region patches of plasma produced elsewhere and F-region arcs (Fig. 4) produced by direct impact excitation by soft electrons (approximately 100 eV). This temporally tracks a 2-D geometric coordinate frame of reference (Figs. 1a and 1b), suggests B_z northward or southward conditions (arcs versus patches, respectively), and provides the desired time history, since the irregularity structure observed at any instant is a consequence of its integrated growth and decay over its lifetime as it moves large distances.

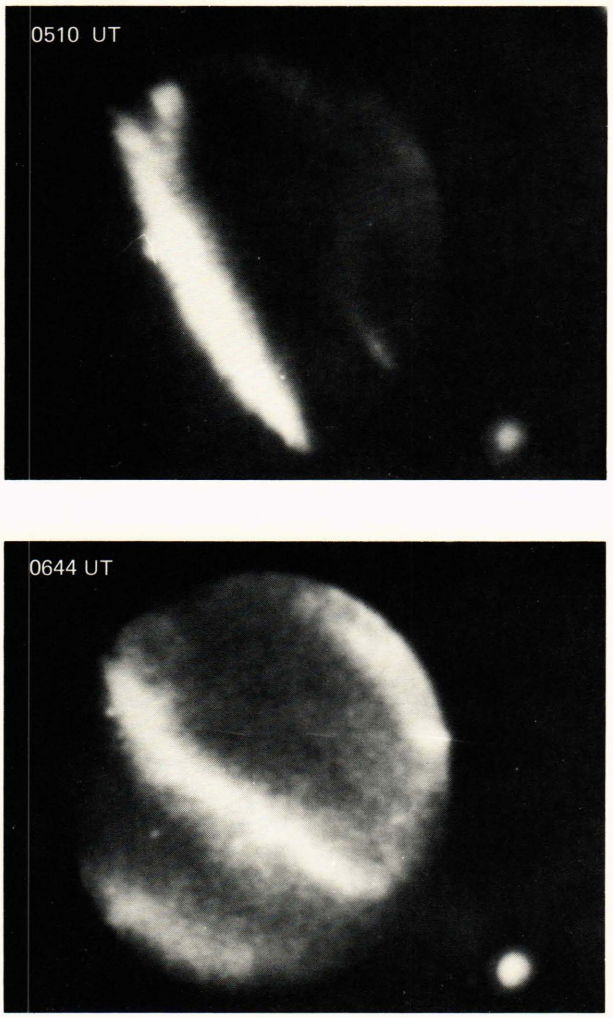

Figure 4 — Sample all-sky imaging photometer pictures of sun-aligned subvisual arcs (E. J. Weber, private communication, 1983).

It has been argued on theoretical grounds[4] that a conducting E layer will play an important role in damping shorter scale structure in the F region. The 2-D history of E-region production can be usefully provided by all-sky image-intensified cameras looking at E-region impact-excitation optical emissions such as 4278 Å N_2^+. This is because electrons with energies much in excess of 500 eV produce ionization at E-region altitudes, where the chemical lifetimes are so short that instantaneous particle fluxes are a good indication of instantaneous E-region ionization and conductivity. Images at 4278 Å thus map E-region ionization rates by harder electrons and, thereby, E-region conductivity.

Electron fluxes are sometimes observed to be sufficiently intense in the 50 to 500 eV range that they can produce significant F-region ionization if maintained for a large fraction of an hour. Softer fluxes produce

so few ions per primary electron that extremely intense fluxes would be required to accumulate such F-region plasma. Images at 6300 Å trace such events.

The Svalbard and mobile aircraft imager can seek plasma intrusion into the polar cap from the winter dark cusp sector. (The colored arc in Fig. 3a is that part of the 75° latitude that is not sunlit in mid-winter). Thule's field of view should intercept virtually all such transpolar plasma transport events, allowing observation of structure downstream of intrusion. This applies to plasma sources, plasma motion, and irregularity evolution. The combined images, with valuable time/area continuity, assume even greater significance in the absence of the vacuum ultraviolet imager on HILAT as a frame of reference within which to order much of the HILAT in situ data.

Fabry-Perot Interferometers. Fabry-Perot interferometers allow sufficiently fine wavelength resolution of atmospheric optical emission lines that thermal broadening (roughly 0.03 Å for 1000 K) can be used to estimate thermospheric temperatures to 5 to 10% accuracy, and bulk Doppler shifts of emission lines (roughly 0.002 Å for 100 meters/second) can be referenced to laser standards to measure thermospheric winds to about ±15 meters/second. Each line-of-sight velocity requires 10 seconds to several minutes of integration as optical intensities diminish from hundreds of Rayleighs (for dense plasma or strong scintillation events) to tens of Rayleighs. A velocity vector requires combining different line-of-sight velocities. Automatic computer-controlled mapping cycles are completed in minutes to an hour for strong-to-weak emissions. The field of view of a pair of Fabry-Perot interferometers with these specifications that will be operating in Thule and Sondre Stromfjord by October 1984 is coincident with the field of view of the all-sky imaging photometers at these sites (shown in Fig. 3a). For conditions changing rapidly in space and time (bistatic), observations of the same volume from two sites are highly desirable. The darker overlap area between Thule and Sondre Stromfjord in Fig. 3a represents the common bistatic field of view for that pair of Fabry-Perot interferometers, allowing instantaneous vector components to be measured. The darker area in Fig. 3b between Svalbard and Kiruna, Sweden, represents the equivalent area that a collaborative effort will afford in the European sector.

Recall that it is the motion of plasma relative to the background atmosphere (**V** − **U**) that is the driving force for some instabilities, as well as the atmospheric drag term that transports moving plasma up **B** to altitudes of negligible, or down to altitudes of rapid, recombination and chemical loss. **U** can exhibit significant spatial and temporal variability (see Figs. 2b and 5).

Radio Beacon Diagnostics

Fluctuations in the integrated electron density deviation of the irregularities along the line of sight between a radio beacon and receiver cause phase and amplitude scintillations of the received radio waves (see, e.g., Fig. 6). Scintillations of satellite radio transmissions provide a measure of the severity of ionospheric irregularities over scale sizes of about 10 km to tens of meters for phase scintillations and of 1 km to tens of meters for amplitude scintillations. The field of view of the HILAT beacon receivers (VHF,ULF, L band) are shown as the smaller solid line ellipses centered on Sondre Stromfjord and Tromso in Fig. 3a. These two ellipses plus one at Thule also approximately contain the field of view of quasi-stationary UHF polar beacons received at these three An L-band receiver for quasistationary Global Positioning System beacons with similar fields of view will also be operated at both Thule and Tromso. Figure 7 illustrates the several-hour time interval over which a

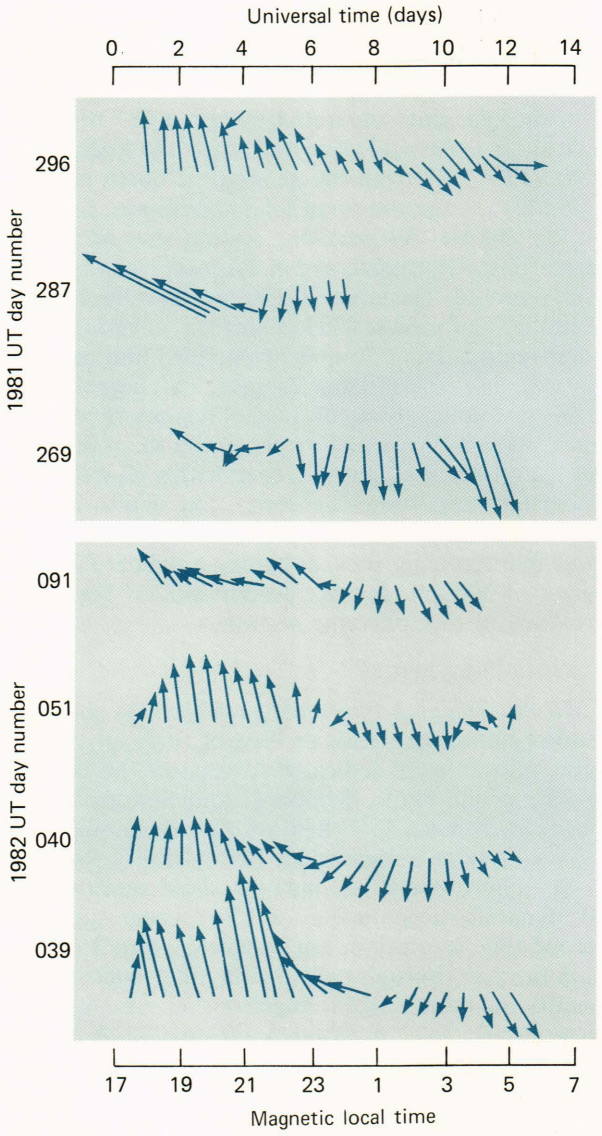

Figure 5 — Observations of the averaged neutral wind vector at Calgary, Alberta, for seven nights in late 1981 and early 1982.[8]

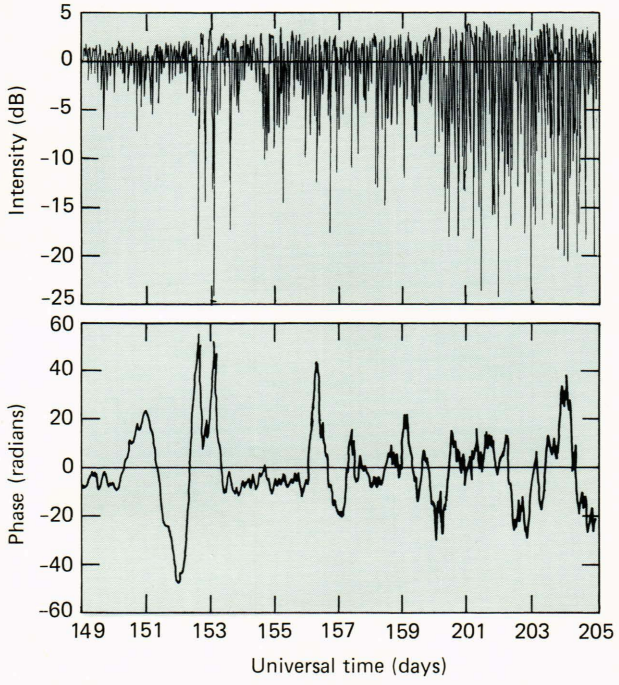

Figure 6 — Time record of 244-megahertz phase and amplitude fluctuations, detrended with a filter cutoff of 0.0067 hertz of the FLEETSAT signal at Goose Bay, Labrador, on March 29, 1979.[3]

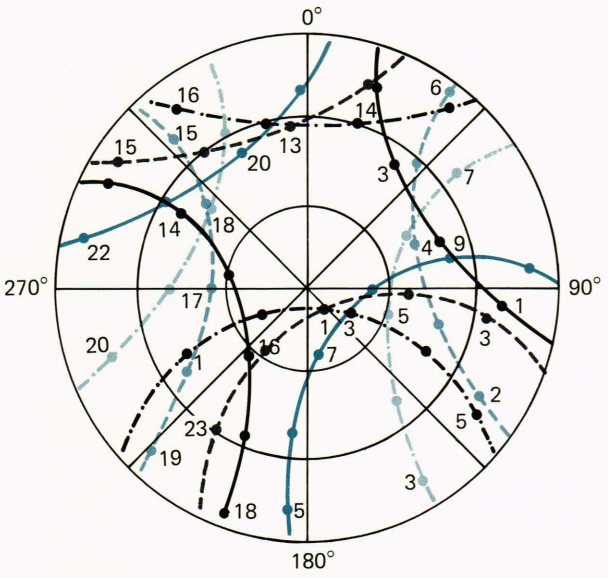

Figure 7 — Visibility of Global Positioning System satellites over Tromso, Norway, versus UT for December 7, 1983. All available satellites are shown on this overplot (J. Klobuchar, private communication, 1983). Dots show the position at hourly intervals between rise and set of the satellite radio beacon.

given beacon slowly drifts across the field of view of a high-latitude receiving site. Each pair of opposite arcs represents the path of a single Global Positioning System satellite; each number along the arc represents the motion of the satellite across the field of view during 2 hours.

Recall that time-continuous measurements are necessary to pursue studies of the tempral evolution of plasma irregularity structure. The receivers that are tuned to quasi-stationary polar UHF and L-band radio beacons at Thule, Tromso, and Sondre Stromfjord (augmented by a mobile beacon on the aircraft) allow placing the instantaneous HILAT flythrough scintillation/in situ data into a time history context. Further, an analysis of the scintillation spectra will provide information regarding the plasma turbulence at the F-region peak, which, in turn, can be compared with the plasma turbulence measured at 830 km altitude by HILAT. Cross-correlation of signals received at pairs of receivers separated by a few hundred meters is also being explored as a potential means of measuring F-region plasma drifts and, thereby, **E**. Cross-correlation of signal strengths received from a radio beacon by pairs of receivers separated by about a few hundred meters ("spaced receivers") defines the degree and orientation of geometric elongations of irregularity structure, as along lines of **B**, surfaces of constant geomagnetic latitude, or plasma convection flow lines.

Radar Diagnostics

Incoherent Scatter Radars. The incoherent scatter radar diagnostic is capable of measurements leading to 26 different ionospheric-thermospheric parameters. The radar echo power is proportional to the number of electrons illuminated by the radar pulse, determined at the measured radar range. The echo Doppler width is a measure of the ion thermal velocity or temperature. The detailed echo spectral shap depends on the electron-to-ion temperature ratio. The echo Doppler shift measures the bulk line-of-sight plasma velocity. Combining different look directions allows construction of a full plasma vector velocity **V**. The four U.S.-supported incoherent scatter radars (Fig. 8) measure **V** in this manner; European incoherent scatter radars (EISCAT and St. Santin, France) measure a common volume (tristatically) from three directions to get instantaneous true vector velocities, particularly desirable at high latitudes. Plasma velocity perpendicular to **B** determines **E** by $\mathbf{V} = \mathbf{E} \times \mathbf{B}$. Plasma velocity parallel to **B** determines the meridional component of neutral wind **U**. Lower altitude (E-region) electron concentration measurements and atmospheric density models allow derivation of conductivities. Conductivity and **E** gradients lead to derived currents.

Spatial resolution varies from 150 meters to hundreds of kilometers along the radar lines of sight (depending on operating modes) and varies across the radar line of sight with the incoherent scatter radars but is nominally one to a few kilometers at F-region altitudes. Time resolution is a few seconds to a fraction of an hour depending on the altitude, latitude, and longitude coverage to be achieved in the observing cycle time.

The fields of view are shown in Fig. 3c for the cusp/polar cap incoherent scatter radars at Sondre Stromfjord; the auroral/plasmapause EISCAT radars at Tromso, Kiruna, and Sodankyla, Finland; and the

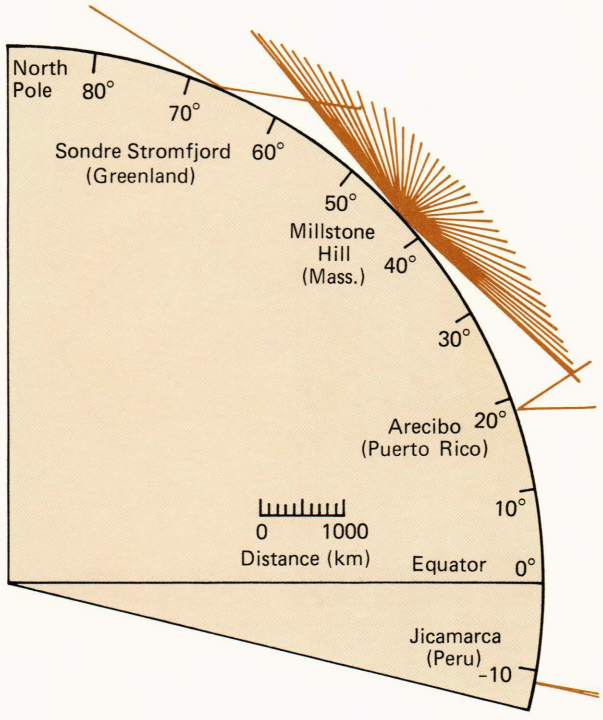

Figure 8 — The four U.S. incoherent scatter radars (V. B. Wickwar, private communication, 1983).

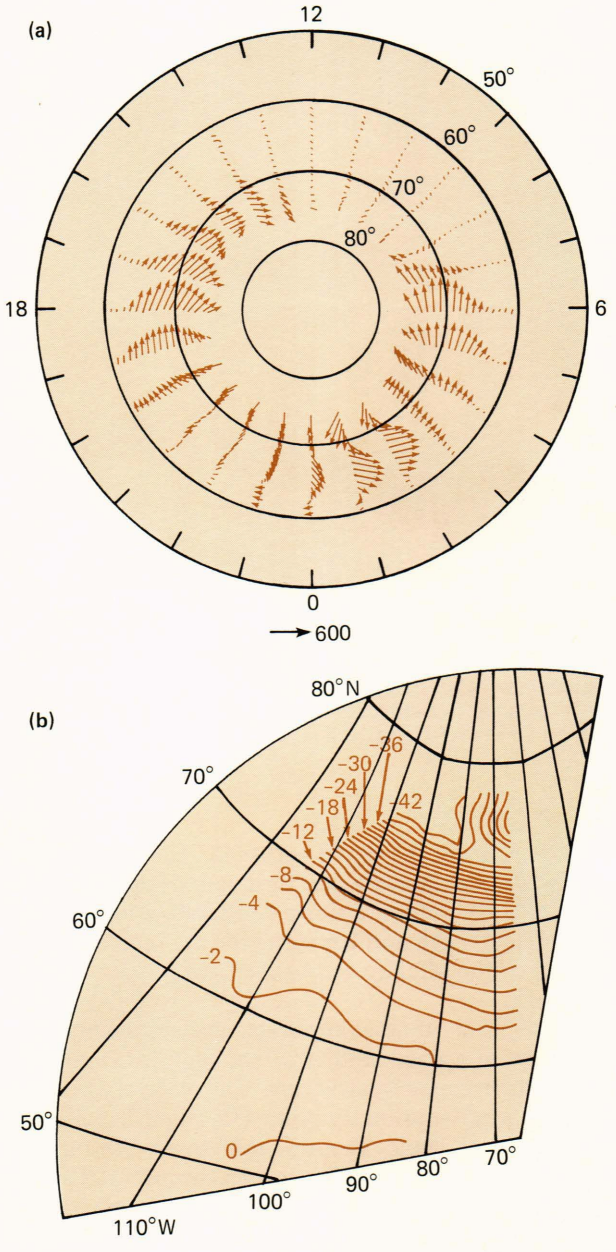

Figure 9 — (a) High-latitude ion velocity data from the Millstone Hill Radar on May 13-14, 1978. The coordinates used are local time-invariant latitude.[7] (b) Maps of the polarization electric field gathered during a substorm on October 13, 1979, by the scanning method. Plot shows the polarization electric field contours as a function of apex latitude and longitude to the west and north of Millstone Hill. Time at the center of the scan is 2184 UT (1629 EST) (J. V. Evans, private communication, 1983).

subauroral radar at Millstone Hill, Mass. EISCAT has an operational tristatic UHF (elliptical field of view) radar and a planned monostatic (rectangular field of view) incoherent scatter radar. The 29° magnetic latitude incoherent scatter radar at Arecibo, Puerto Rico, and the magnetic equatorial incoherent scatter radars at Jicamarca, Peru, are not shown in Fig. 3c but are included in Fig. 8, which shows the angular overhead field of view of the U.S. longitude chain of incoherent scatter radars up to the HILAT orbital altitudes.

Figure 9a illustrates ion velocity data derived from the Millstone Hill incoherent scatter radar for a representative 24-hour period. The data span 50° to 75° magnetic latitude; combining this with Sondre Stromfjord incoherent scatter radar data will extend coverage to 80° magnetic latitude. While this format and time resolution show the gross features of Fig. 2a, they mask shorter time scale fluctuations in **V** and **E** known to be important. This same information can be presented in the form of contours of ionospheric potential. Figure 9b shows the plasma convection pattern in the form of a map of a polarization electric field during a substorm. Scanning the Millstone Hill radar antenna in azimuth spanned this 25° of latitude and 5 hours of local time in less than 10 minutes. (The complementary strength of VHF STARE and SABRE type radars will be discussed shortly.)

Figure 10 illustrates contours of electron concentration versus altitude and latitude, measured by an auroral incoherent scatter radar at Chatanika, Alaska at consecutive 14-minute intervals. These are extracted from a full set spanning sunset through midnight, which verifies the temporal and longitudinal persistence of the strong plasma enhancement seen 100 to 400 km north of the incoherent scatter radars, above the diffuse auroral E region. Coincident north-south aircraft flights carrying a receiver tuned to a UHF satellite radio beacon established a sharply defined

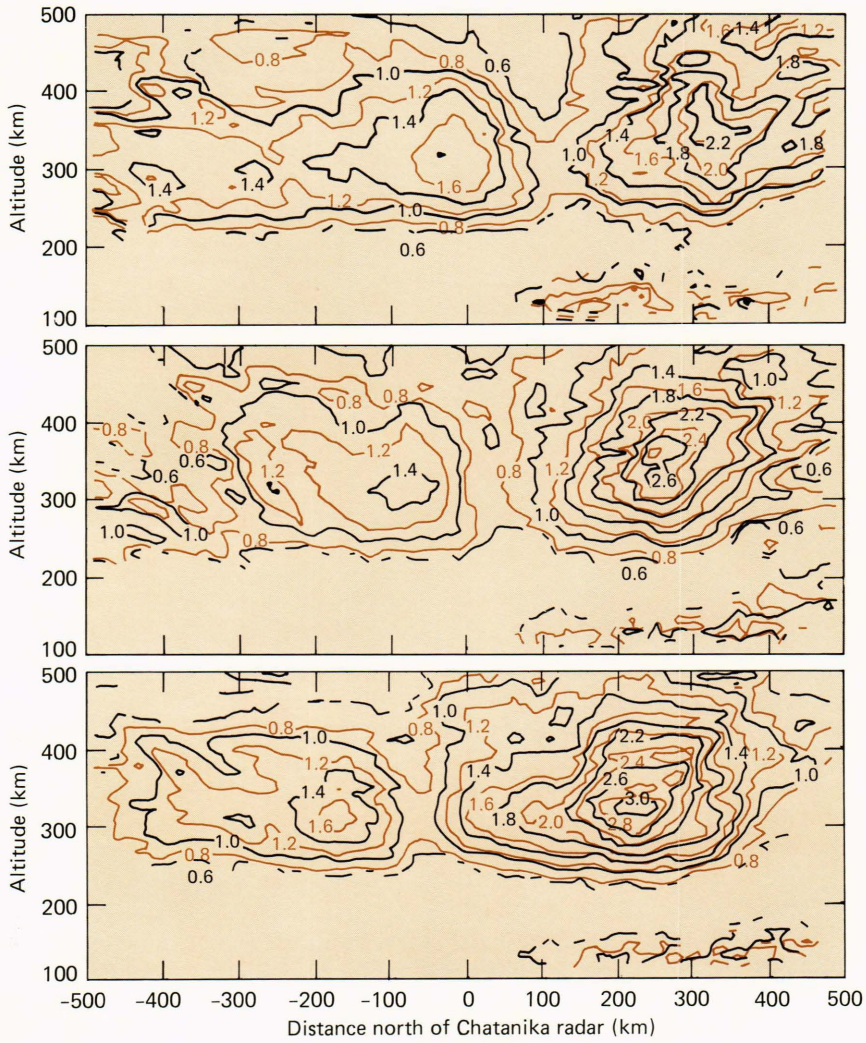

Figure 10 — Contours of constant electron concentration on a latitude-longitude grid identify pre-existing F-region plasma as a persistent source of severe auroral region scintillation.[9]

boundary to the edge of this plasma enhancement, inside of which severe scintillation was produced. Contours such as these can be produced in about half this observing cycle time at Sondre Stromfjord and in comparable time by EISCAT.

The ability of the incoherent scatter radars to measure altitude and latitude profiles, to sample spatial areas or volumes with time continuity, and to map temporal evolution of plasma concentrations, electric fields, currents, winds, and conductivities (as well as gradients in these quantities) renders it an exceptionally powerful diagnostic for quantitatively testing many theories of direct concern to the HILAT mission.

Coherent Radars. VHF Doppler radars offer the powerful capability of high spatial and temporal resolution of **E** measurement over about a 500 × 500 km latitude-longitude grid whenever **E** exceeds the threshold of about 15 millivolts/meter (**V** exceeds about 300 meters/second). Above these threshold values of **E**, auroral irregularities cause backscatter echoes whose Doppler shift can now be theoretically related to the bulk plasma velocity field. Resolution for the STARE and SABRE solid line field of view shown near Scandinavia in Fig. 3b is 20 × 20 km and 20 seconds. An example of 20-second resolution measurement of a rapidly changing **E** is shown for the SABRE radar in Fig. 11. Mean values, shears, and temporal evolution of **E** over an area this large is again of obvious value to studies of the temporal evolution of plasma irregularity structure, including testing of growth and decay rates. Radio beacon receivers will be operated with time-continuous scintillation data within the SABRE and STARE fields of view, on occasion simulaneously threaded by snapshot HILAT passes. Similar studies can be done by combining the Canadian Bistatic Auroral Radar System (a VHF radar near Churchill, Manitoba) with the Canadian HILAT receiver. The Bistatic Auroral Radar System field of view is also shown in Fig. 3b. Echoes are received only perpendicular to **B**, so high-latitude VHF echoes are confined by geometry to E-region altitudes. To achieve perpendicularity at F-region altitudes requires going to HF frequencies, which can refract to become perpendicular to **B**.

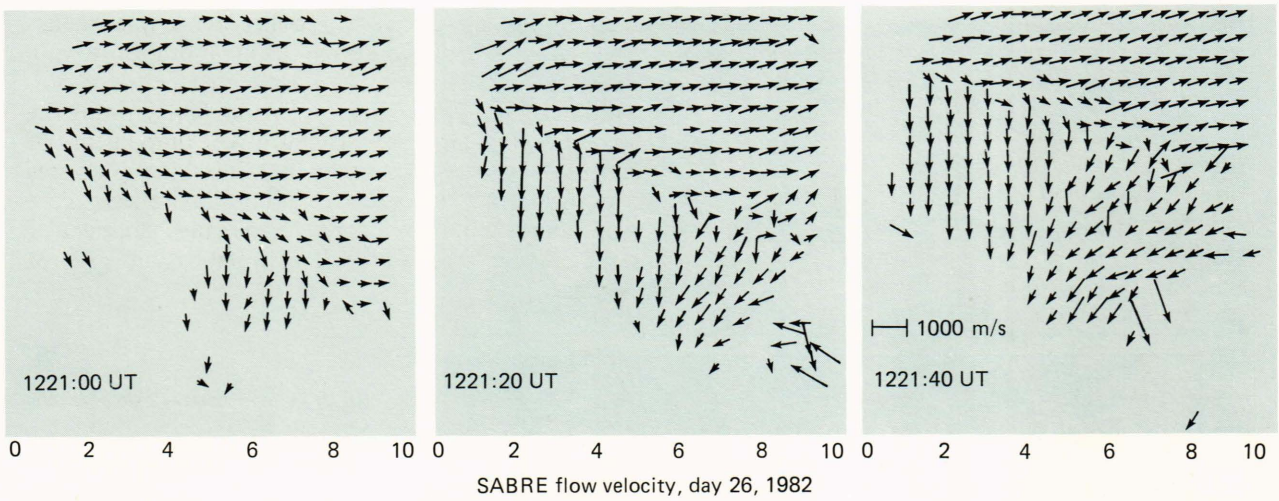

Figure 11 — Plasma flow velocities on a latitude-longitude grid measured with 20-second time resolution (T. Jones, private communication, 1983).

HF Doppler radars have also been constructed to measure backscattered echoes from small-scale ionospheric irregularity structure at high latitudes. Fields of view of one radar north of Goose Bay, Labrador, and two operated in mid- and northern Europe (EDIA and SARARI, respectively) are shown by dashed lines in Fig. 3b. The strength of such studies is that scattering is by small-scale irregularities (approximately 7 to 20 meters). They complement the larger scale diagnostics very well and allow studies tracing cascading and wavelength-coupling theories. They also promise plasma-convection information over relatively large areas with resolutions of a few tens of kilometers and on the order of a minute. A theoretical consideration is that we do not yet know what mechanisms cause the F-region irregularities that backscatter the high-frequency signals. Also there are attendant uncertainties in the relationship between drift velocities of the small-size irregularities (about 10 meters) sensed by scintillation spaced receivers (about 1 km), and the bulk plasma flow sensed by incoherent scatter radars, satellite driftmeters, or Fabry-Perot interferometers observing 7320 Å emissions. Coincident HILAT and complementary data should illuminate such questions to allow fuller application of this diagnostic. A technical consideration is that the backscatter echoes are obtained only because of high-frequency refraction in the ionosphere (allowing bending of the high-frequency waves to become perpendicular to **B** in the F region). This leads to some attendant uncertainty in determining where the echoes come from.

Airborne Diagnostics

The Air Force Geophysics Laboratory's Ionospheric Airborne Observatory is outfitted with HILAT radio beacon receivers as well as receivers for quasi-stationary high-latitude radio beacons. Use of the latter for "painting" those portions of slowly moving plasma enhancements producing severe scintillations has already been noted in connection with Fig. 10. For HILAT passes seeking to relate in situ data at 830 km to radio beacon sensed irregularities along the same **B** at 300 km, a ground-based station will have its line of sight to the satellite penetrate the F region within 50 km of the same **B** as the in situ data (many high-latitude features of concern are on the order of 100 km wide) only once or twice per month. In this sense, a single aircraft flight may acquire "several months" worth of true coincidences within a geophysically brief span of time.

By October 1984, the aircraft will be outfitted with upgraded optical equipment including a photometer, spectrometer, and all-sky imaging photometer. The six-channel meridian scanning photometer (with a 10 Rayleigh threshold sensitivity) can scan a 160° meridian slit field of view in 1 minute (10 samples per second), each point with a variable 0.5 to 3° field of view. The spectrometers, also with about a 10 Rayleigh threshold sensitivity, will have a vertical 5° field of view and will span 3700 to 8000 Å (with roughly a few angstroms resolution) at a computer-controlled variable rate, including jump-and-scan over several lines. The all-sky imaging photometer was discussed earlier and most notably will be upgraded to a 10^5 dynamic range to allow its wide field of view (1200 km for F-region emission; see shaded areas of Fig. 3a) to simultaneously observe weak airglow and strong auroral features. This will be particularly useful when features such as those identified in Figs. 1a and 1b are close to "merging" with the auroral oval, or when sun-aligned features (Fig. 1a) may suddenly "brighten."

The aircraft also carries a high-frequency Doppler radar capable of discriminating high-frequency echoes by signal strength, Doppler, and polarization. This discrimination has allowed plasma density profiles and Doppler velocities to be obtained with unprecedented reliability from even highly structured plasma features such as the strongly scintillating F-region patches (Fig. 1b).

This airborne (earth-bound) observatory can be placed on any major runway or in any unrestricted airspace around the globe.

Composite Diagnostics

Patterns of motion of direct concern to the HILAT mission are identified in Figs. 1 and 2. Fields of view of optical, radio, and radar facilities of direct concern to the HILAT mission are shown in Fig. 3. Representative direct observations of bulk ionospheric plasma and thermospheric flow by such facilities are given in Figs. 5, 9, and 11. Observations of regions of strong plasma structuring are discussed with reference to Figs. 4, 6, and 10.

The bulk-density history calls for definition of the dynamic high-latitude plasma "convective pattern," an example of which is shown in Fig. 2a, as well as of high-latitude plasma-enhancement patterns, as noted in Fig. 1. The time-space history for the convection pattern can be obtained by combining HILAT with high-latitude incoherent scatter radars or other **E**-measurement stations (selected coherent radars, Fabry-Perots, and spaced radio-beacon receivers), and for the enhancement patterns by a network of all-sky image-intensified optical sensors discussed later. Both requirements are for time continuity of measurement over a large area, currently available only from ground-based diagnostics.

The degree of structuring (approximately 100 km to submeter) within the bulk plasma requires time-space history of that region of plasma. This is best provided (for **E** greater than 15 millivolts/meter) by time-continuous area coverage of coherent Doppler radars (particularly VHF) to define the evolution of driving **E** fields, supplemented by time-continuous quasi-stationary radio-beacon scintillation data defining the evolution of irregularity structure. The time-history of calculated growth rates for various instability processes can further be addressed by adding simultaneous time continuous incoherent scatter radar measurement of gradients in n_e, **E**, and **I**, augmented by Fabry-Perot **U** data.

REFERENCES

[1]E. J. Weber and J. Buchau, "Polar Cap F Layer Auroras," *Geophys. Res. Lett.* **8**, 125 (1981).

[2]J. Buchau, B. W. Reinisch, E. J. Weber, and J. G. Moore, "Structure and Dynamics of the Winter Polar Cap F Region," *Radio Sci.* **18**, 995-1010 (1983).

[3]S. Basu. E. MacKenzie, H. C. Carlson, D. A. Hardy, F. J. Rich, and R. C. Livingston, "Coordinated Measurements of Low-Energy Electron Precipitation and Scintillations/TEC in the Auroral Oval," *Radio Sci.* **18**, 1181-1187 (1983).

[4]J. F. Vickrey and M. C. Kelley, "The Effects of a Conducting E-Layer on Classical F-Region Cross-Field Plasma Diffusion," *J. Geophys. Res.* **87**, 4461 (1982).

[5]R. A. Heelis, J. K. Lowell, and R. W. Spiro, "A Model of the High-Latitude Ionospheric Convection Pattern," *J. Geophys. Res.* **87**, 6339-6345 (1982).

[6]R. G. Roble, R. E. Dickinson, and E. C. Ridley, "Global Circulation and Temperature Structure of the Thermosphere with High-Latitude Plasma Convection," *J. Geophys. Res.* **87**, 1599 (1982).

[7]J. V. Evans, J. M. Holt, W. L. Oliver, and R. H. Wand, "Millstone Hill Incoherent Scatter Observations of Auroral Convection over $60° \leq \Lambda \geq 75°$; 2. Initial Results," *J. Geophys. Res.* **85**, 41 (1980).

[8]J. W. Meriwether, "Observations of Thermospheric Dynamics at High Latitudes from Ground and Space., *Radio Sci.* **18**, 1035-1052 (1983).

[9]E. J. Weber, J. Buchau, H. C. Carlson, Jr., D. A. Hardy, J. F. Vickrey, R. R. Robinson, and D. J. Strickland, "Coordinated Radio and Optical Measurements of the Auroral E and F Layers (abstract)," *EOS Trans. Am. Geophys. Union* **64**, 777 (1983).